polymer papers

The structure of the mesomorphic phase of quenched isotactic polypropylene

V. Caldas and G. R. Brown*
Department of Chemistry, McGill University, 801 Sherbrooke Street W., Montréal, Québec, H3A 2K6, Canada

and R. S. Nohr and J. G. MacDonald
Kimberly-Clark Corp., 1400 Holcomb Bridge Road, Roswell, GA 30076, USA

and L. E. Raboin
Polymer Science and Engineering, University of Massachusetts, Amherst, MA 01003, USA
(Received 5 December 1992; revised 16 June 1993)

Scanning transmission electron microscopy (STEM) dark field images reveal that within the essentially amorphous matrix of quench-cooled isotactic polypropylene (iPP) there exist microcrystalline regions, 100 to 200 Å in size, that have the α-monoclinic crystal form ($a=6.67\pm0.01$, $b=20.89\pm0.05$, $c=6.48\pm0.01$ Å, $\beta=98.4\pm0.6°$). Regions of lower crystalline order are also observed which, according to micro–micro diffraction, also possess the α-monoclinic crystal structure but with substantially larger unit cell constants ($a=7.03\pm0.01$, $b=21.1\pm0.1$, $c=6.47\pm0.02$ Å, $\beta=99\pm2°$). Differential scanning calorimetry studies indicate that during quench cooling to the glassy state iPP samples attain a low degree of crystalline order to an extent that depends on sample mass. Upon heating from the glassy state, these samples exhibit exothermic transitions, between −15 and 120°C, that correspond to the formation and subsequent perfection of the microcrystalline regions observed by STEM dark field.

(Keywords: polypropylene; morphology; crystallization)

INTRODUCTION

Since the initial disclosure by Natta *et al.*[1] that propylene could be polymerized to yield high molecular weight, isotactic semicrystalline polymers, there have been numerous studies on the structure, morphology, mechanical properties and their interrelationships. To a considerable degree, this intense interest has resulted from the widespread industrial applications for this polymer. Within this large body of literature there is particular emphasis on the effects of thermal history and mechanical deformations on the crystalline morphologies of polypropylene (PP). The morphology of a partially ordered phase that is attained as a result of quench cooling an isotactic polypropylene (iPP) sample is the focus of this study.

When crystallized either from the melt or from solution, iPP adopts a 3_1 helical conformation. Depending on the crystallization conditions[2–8], these helices pack in different geometries giving rise to the three well known polymorphs of iPP[9], namely the α-monoclinic, the β-hexagonal and the γ-triclinic crystal forms, which exist in conjunction with an amorphous phase. It was pointed out many years ago[10–12] that a phase possessing order intermediate between the amorphous (atactic) and crystalline states can be obtained by quench cooling. Although the X-ray scattering curve for the quench-cooled sample is very similar to that for atactic PP, the presence of a second scattering maximum at 22.2° suggests the existence of a somewhat greater degree of order. Infra-red studies[13] of the quenched phase yielded spectra very similar to that of the α-monoclinic crystalline form, indicating the existence of the same 3_1 helical conformation. In addition, the helices have a parallel orientation and the packing perpendicular to their axes is more disordered than along the axes. Since the packing of the helices does not appear to be completely random, Natta *et al.*[10] referred to this partially ordered phase as a 'smectic' form, indicating a degree of order higher than molecular parallelism found in a nematic liquid crystalline phase.

Following the initial description of the quenched phase of iPP as being a 'smectic' modification, much work gave evidence that it possessed higher levels of order. Wyckoff[12] found a certain degree of correlation between adjacent helices, suggesting short-range three-dimensional order of a limited nature. Miller[13] and subsequently Zannetti *et al.*[14] described the quenched iPP morphology as paracrystalline in the sense of Hosemann[15], i.e. having statistical variations of the edges of the unit cell in both length and direction.

Gailey and Ralston[16] suggested that the partially ordered phase of iPP is composed of small hexagonal crystals that are 50–100 Å in size. This proposal was based solely on the observation that the two diffraction maxima obtained for the quenched phase coincide with the two most intense diffraction maxima of the hexagonal phase. Farrow[17] agreed with the concept of fine crystals but did

*To whom correspondence should be addressed

0032-3861/94/05/0899–09

not make reference to a hexagonal morphology. Electron microscopy studies of the morphology of the quenched phase, carried out by Gezovich and Geil[18], revealed 'ball-like' structures about 125 Å in size, and they suggested that these were defective hexagonal crystals. On the other hand, Bodor *et al.*[19] assumed the quenched phase to be composed of small crystals of the monoclinic form and suggested that the characteristic X-ray scattering pattern is due to crystal size line broadening. Finally, McAllister *et al.*[20] proposed that the polymer chains in the quenched phase are arranged in a square symmetry and estimated a crystal size of approximately 30 Å. This was disputed by Guerra *et al.*[21], who contended that all of the reflection maxima were interpreted as equatorial reflections, which does not agree with the X-ray pattern of oriented quenched samples.

To attempt a theoretical elucidation of the structure of the partially ordered phase of iPP, Corradini *et al.*[22,23] compared the experimentally determined X-ray diffraction intensities for this phase with calculated Fourier transforms for various models of chain aggregates packed in the α-monoclinic and β-hexagonal crystal forms, as well as for disordered models possessing character of both phases. The local correlation between chains was found to more closely resemble the crystal structure of the α-monoclinic crystal form than the β-hexagonal, although any correlation between chains appeared to be lost at distances of the order of 30–40 Å.

Although the degree or type of order in the quenched phase of iPP has not been fully determined, Hsu *et al.*[24], through X-ray diffraction and electron microscopy studies, have found that the 'smectic' morphology develops as the quench-cooled sample is heated between −20 and 0°C, i.e. it results due to crystallization from the glassy state. Differential scanning calorimetry (d.s.c.) studies confirmed that upon heating a quench-cooled sample of iPP, crystallization occurs in the same temperature region where the morphological changes were observed by electron microscopy. Infra-red spectra obtained by Glotin *et al.*[25] also present evidence that quench-cooled iPP crystallizes from the glassy state.

The goal of this work was to obtain a better understanding of the morphology of the quenched phase of iPP. To this end, electron microscopy techniques, offering higher resolution than techniques used previously, were employed to probe the local order, i.e. areas less than 100 Å^2. Detailed d.s.c. studies are also presented, which yield a fuller description of the formation of this phase, i.e. about the crystallization from the glassy state.

EXPERIMENTAL

The iPP used in this study was obtained from Exxon (Exxon 3445, melt flow index = 34). Its weight- and number-average molecular weights, as obtained through gel permeation chromatography (g.p.c.) analysis, were 39 800 and 135 500, respectively, referenced to narrow molecular weight PP standards in 1,2,4-trichlorobenzene at 145°C. Samples of the mesomorphic form were prepared by melting the iPP sample between microscope slides at a temperature of 225°C for 15 min, followed by quench cooling in a cold medium, namely a dry ice/acetone slush (−78°C) or a pentane slush (−130°C). An aluminium spacer of 14 μm between the microscope slides controlled the sample thickness. The mesomorphic phase was characterized by electron microscopy, solid state nuclear magnetic resonance (n.m.r.) with cross polarization/magic angle spinning (CP/MAS), and d.s.c.

Electron microscopy

The previously quench-cooled iPP films were prepared for electron microscopy in the following manner: The film was cut into a square, about 5 mm × 5 mm, and embedded in Spurr epoxy resin. The epoxy was cured at room temperature for 1 week, after which the sample was trimmed in preparation for microtoming using the FC4 Reichert-Jung cryo-ultramicrotome set at a temperature of −65°C. Thin sections, about 400 Å in thickness, were collected and mounted on 3 mm 600 mesh hexagonal grids. The samples were then transferred to the Jeol cryo specimen holder and observed with a Jeol 100cx STEM electron microscope. During the observations the samples were kept at liquid nitrogen temperature to minimize electron beam damage.

To avoid damage to the entire grid sample, the scanning electron beam was controlled using the microscope electron optics to view only specific areas. The scan generator reduced the incident beam to a minimal spot size of 15 Å before the specimen plane, thus allowing the scan width and length on the grid to be controlled by the operator. By using the beam stop below the specimen plane, dark field images (n-beam) of selected specimen areas were obtained using the electrons scattered by the microcrystalline areas. High speed photographic film (400 ASA) was used to record the images. In addition, a beam blanking device, located in the condenser lens beam tilt circuitry, and a minimum dose device were used to minimize electron beam damage. The blanking device allowed rapid tilting of the beam off and on the optical axis, thus accomplishing very fast exposure times. By use of the minimum dose device the beam could be focused on an adjacent area after which it was exposed on a selected new area which had not yet been damaged. In this study, imaging was done near the copper grid bars so that much of the electron beam heating was conducted away from the area of interest. Separate experiments using a thermocouple revealed heating to temperatures no higher than 50°C in the time required to record the dark-field image.

Micro–micro electron diffraction patterns were also obtained using the Jeol 100cx STEM microscope, which made it possible to record diffraction patterns of crystalline areas much smaller than could be viewed by conventional TEM. Making use of the 'spot' mode (15 Å) in selected area scanning, microdiffraction patterns were obtained for selected areas of the quench-cooled film. The condenser and intermediate lenses were controlled manually, thus allowing for different camera lengths. The final camera length was determined using a gold standard. To minimize sample beam damage and co-operative molecular rearrangement due to the electron bombardment, Kronex X-ray film was used to record the diffraction patterns, which decreased exposure times to the order of 2 s. Microdiffraction patterns probing areas less than 100 Å^2 were recorded. In the calculation of the unit cell constants, two to five diffraction patterns were obtained for the area of interest for each different crystal orientation. Three to six unit cell dimensions were calculated and averaged.

Solid state n.m.r. experiments

CP/MAS ^{13}C n.m.r. spectra were recorded at room

temperature with a Chemagnetics CMX-300 spectrometer operating at a static field of 7.1 T. The samples were spun at the magic angle at a frequency of about 3.8 kHz in a 7.5 mm o.d. zirconia rotor. A contract time of 1 ms was used in the cross polarization, with a pulse delay of 3 s. A 62.5 kHz r.f. decoupling field was used with a decoupling period of 200 ms. All spectra were referenced to tetramethylsilane in a spectral window of 30 kHz by setting the methyl resonance of hexamethyl benzene to 17.40 ppm. Previous to Fourier transformation, the f.i.d. was zero-filled to 4 K. Spin-lattice relaxation times in a rotating frame, $T_{1\rho}(^1H)$, were measured for the methylene, methine and methyl carbons by varying an interval, τ, before cross polarization. The relaxation times were obtained by fitting the intensity data on a double exponential decay curve using a computer program (Peakfit, obtained from Jandel Scientific).

Differential scanning calorimetry

Thermal analysis was performed with a Perkin–Elmer DSC-7C by heating the sample at 20°C min^{-1} from −60 to 220°C under a nitrogen flow. Calibration of the d.s.c. for temperature and enthalpy was accomplished by running two high purity standards, namely indium and octadecane. All of the annealing experiments were performed by heating the sample to the appropriate temperature at a rate of 20°C min^{-1}, and maintaining this temperature for the desired time. The sample was then cooled at 100°C min^{-1} (nominal) to −45°C and allowed to come to thermal equilibrium previous to thermal analysis.

To describe the crystallization process from the glassy state, the iPP sample in the aluminium d.s.c. pan must be quench cooled and maintained cold until thermal analysis. This was accomplished by the following technique. The d.s.c. pan containing the iPP sample was heated to 220°C and maintained for 15 min. It was then transferred into a Dewar flask containing a pentane (h.p.l.c. grade) slush, thus quench cooling the sample to −130°C. The sample pan was then transferred to a small flat-bottomed glass vessel containing a small amount of pentane kept at −78°C by immersing the glass vessel in a dry ice/acetone slush. The vessel, which was maintained at −78°C, was then attached to a vacuum line pumped by a mercury diffusion pump for at least 4 h to remove the pentane. It was then flushed with cold, dry nitrogen, removed from the vacuum line, and the clean d.s.c. pan was quickly transferred into a Dewar flask containing liquid nitrogen. The sample was then transferred to the d.s.c. sample holder, which was maintained at −60°C by the Perkin–Elmer intracooler accessory, allowed to come to thermal equilibrium and subsequently analysed as described above.

RESULTS AND DISCUSSION

Differential scanning calorimetry

Quench-cooled samples maintained at room temperature. *Figure 1* shows the d.s.c. thermogram for the heating of an iPP sample which was allowed to warm to room temperature after being quench-cooled in a dry ice/acetone slush at −78°C. In addition to the large endotherm between 120 and 165°C, which corresponds to the melting of the developed crystalline morphology, two distinct regions characterize the thermal behaviour of this quenched phase. The first is a small endotherm, of

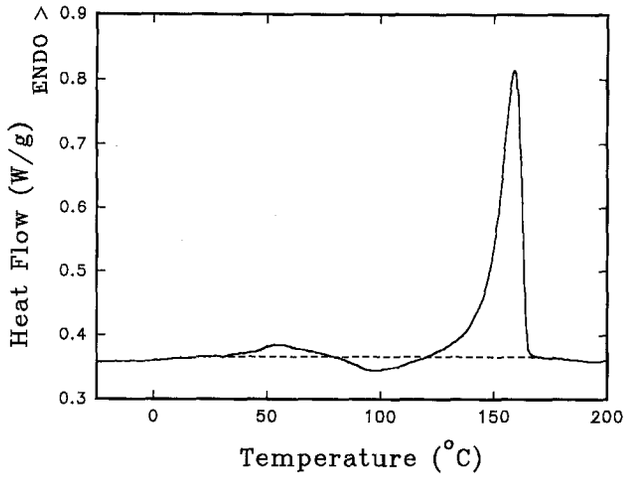

Figure 1 D.s.c. thermogram of an iPP sample quench cooled in a dry ice/acetone slush at −78°C and allowed to return to room temperature. The dashed line represents the baseline used in the separation of endothermic and exothermic regions

area corresponding to 4.4 J g^{-1}, in the interval between 30 and 75°C, which is very similar to that observed previously by Fichera and Zannetti[26] for quenched iPP samples subjected to a low temperature anneal. They ascribed it to the melting of small crystals formed during annealing. Grebowicz *et al.*[27] confirmed the existence of this endothermic transition in annealed quenched samples but demonstrated that it also occurs for a quench-cooled sample that has not been annealed. They also attributed it to the melting of small crystals formed during the quenching process. The nature of this endotherm will be discussed further once the morphology of this quenched phase has been described.

As reported previously[26–29], the low temperature endotherm is followed by an exothermic transition in the interval between 80 and 120°C, which has been attributed to a transition from a quenched phase morphology to the stable α-monoclinic crystalline phase. This interpretation was based on X-ray evidence[30] which showed a transformation from two broad diffraction maxima, the characteristic diffraction pattern of the quenched phase, to the usual diffraction pattern of the crystalline α-monoclinic phase that becomes evident for samples annealed at temperatures ≥60°C. The heat of conversion is −8.8 J g^{-1} (−2.1 cal g^{-1}), or approximately 50% of that reported by Fichera and Zannetti[26]. It is similar to, but slightly greater than, that obtained by Grebowicz *et al.*[27], who reported a value 25–33% of that reported by Fichera and Zannetti. The discrepancy with the value of Grebowicz *et al.* may reflect different quenching techniques, which could result in differences in the morphology. In the work of Fichera and Zannetti, the thermograms begin at 50°C which, as seen in *Figure 1*, is well into the low temperature endotherm and consequently results in a misplaced baseline. This exotherm will also be discussed further in light of new electron microscopy results as well as d.s.c. experiments presented below.

The d.s.c. thermograms for various quench-cooled iPP samples that have been annealed subsequently for 40 min at different temperatures, are shown in *Figure 2*. The low temperature endotherm that begins near 40°C for the unannealed quenched sample shifts to higher temperature with increasing anneal temperature, as shown in *Figure 3*.

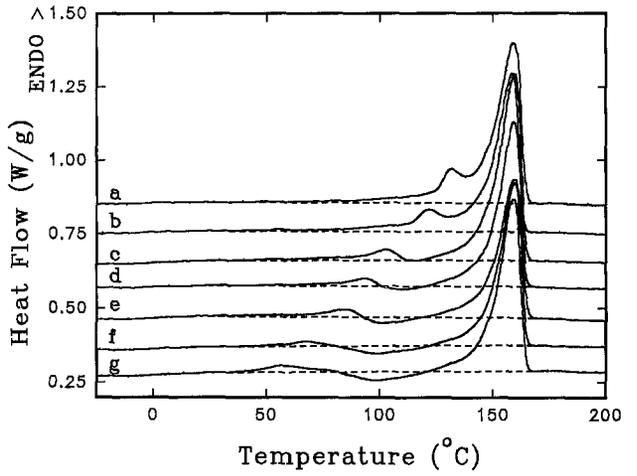

Figure 2 D.s.c. thermograms of iPP samples quench cooled in a dry ice/acetone slush and subsequently annealed for 40 min at (a) 120, (b) 110, (c) 90, (d) 80, (e) 70, (f) 50, (g) 30°C. The dashed lines represent the baselines used in the separation of endothermic and exothermic regions

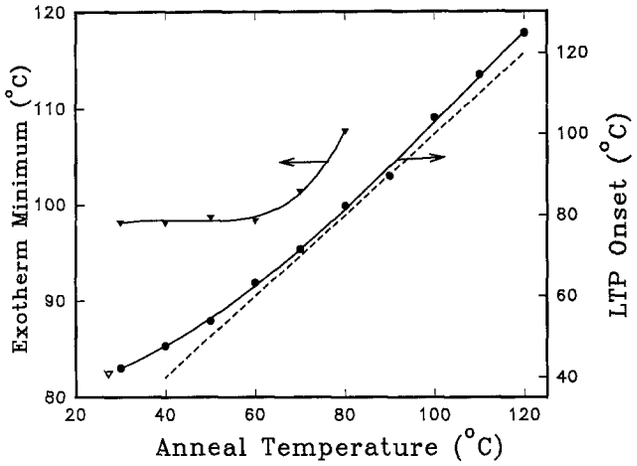

Figure 3 Effect of anneal temperature on the onset of the low temperature peak (LTP) and on the exothermic transition. The dashed line reflects the relationship $T_{onset} = T_{anneal}$

Although previous studies[26,27] reported that the onset of this endotherm corresponds to the anneal temperature, deviations from such a linear relationship are observed at anneal temperatures below 60°C and again at the higher temperatures, i.e. above 100°C. For the quench-cooled sample which has not been annealed, the onset temperature of the endotherm (indicated by the inverted open triangle in *Figure 3*) occurs at 42°C. In keeping with the non-linear relationship represented in *Figure 3*, this onset temperature for the low temperature endotherm corresponds to an anneal temperature of 27°C. Therefore, the quench-cooled sample that was allowed to return to room temperature has a crystalline morphology which is consistent with that expected for a sample annealed at room temperature. If this endotherm represents the melting of an imperfect crystalline morphology, as suggested previously, such crystals must develop at a lower temperature, as concluded by Hsu *et al.*[24].

This endotherm remains approximately constant in area, varying randomly between 3.6 and 5.2 J g^{-1}, for anneal temperatures between 30 and 80°C. It is difficult to accurately determine the ΔH for samples annealed at temperatures above 100°C, because the low temperature peak coalesces into the onset of the main melting endotherm. Fichera and Zannetti[26] reported an increase in the size of this low temperature endotherm with increase in temperature, between 70 and 120°C, as well as with anneal time. However, as described above, those areas are in doubt because of misplaced baseline.

The exothermic transition at about 100°C can be discerned only for samples that have received thermal treatments at 90°C or lower, as seen in *Figure 2*. The minimum of this peak remains at 98°C for anneal temperatures ≤60°C (*Figure 3*) and the magnitude of its area remains constant at about −8.0 J g^{-1}. Higher anneal temperatures result in a small shift to higher temperature as well as a rapid decrease in its magnitude until it disappears at anneal temperatures ≥90°C.

Quench-cooled samples maintained at low temperature. D.s.c. thermograms of 'as-quenched' iPP samples, i.e. samples which have been quench cooled and maintained at low temperature until analysis, are shown in *Figure 4*. In each case the baseline, represented by a dashed line, used in the separation of exothermic and endothermic regions, is an extension of the baseline obtained for the melt back to the point where it intercepts the thermogram at about −16°C, i.e. at the end of the glass transition. Upon heating, the samples exhibit a glass transition at −19 ± 1°C followed by an exothermic peak, with an onset at about −14°C, due to crystallization from the glassy state. The thermogram remains exothermic up to 120°C, in keeping with the occurrence of crystallization or recrystallization processes. Although Hsu *et al.*[24] also detected a crystallization peak upon heating the quench-cooled iPP sample, the exothermic region of the thermogram between room temperature and 120°C was not detected, possibly due to baseline curvature which is evident in their thermogram.

The d.s.c. thermograms shown in *Figure 4* for the two samples of iPP weighing 1.96 and 4.22 mg have identical glass transitions, crystallization and final melting temperatures, as well as final heats of fusion. However, the sample of lower mass has a substantially larger change in heat capacity at the glass transition, as well as a larger heat of crystallization, as measured in the region between −15 and 120°C.

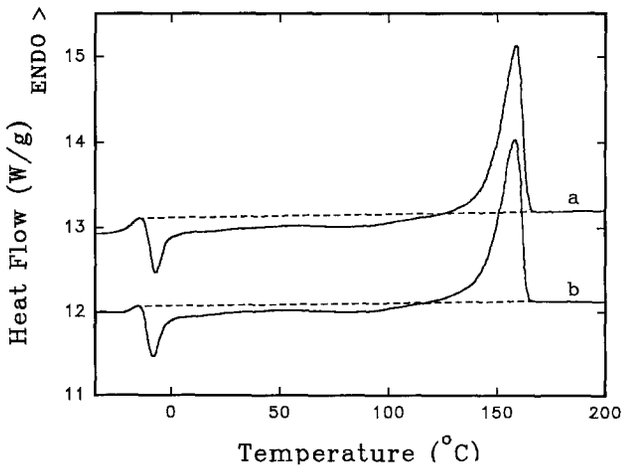

Figure 4 D.s.c thermograms of iPP samples, with weights of (a) 1.96 mg and (b) 4.22 mg, quench cooled in a pentane slush (−130°C) and maintained cold until thermal analysis. The dashed line represents the baseline used in the separation of endothermic and exothermic regions

Table 1 Transition temperatures and per cent crystallinity as obtained from excess endothermic energy and change in heat capacity from d.s.c. thermograms for 'as-quenched' iPP samples of various weights

Weight (mg)	Transition temperature (°C)			Excess energy ($J g^{-1}$)	% Crystallinity	ΔC_p ($J g^{-1} °C^{-1}$)	% Crystallinity
	T_m	T_c	T_g				
7.85	157.5	−7.0	−18.6	31	19	0.22	60
5.25	160.6	−6.4	−16.9	29	18	0.23	58
4.22	157.5	−8.5	−19.2	30	18	0.27	52
2.80	158.6	−7.4	−19.3	20	12	0.36	36
1.96	158.7	−7.5	−19.0	11	6.5	0.50	11
1.30	157.3	−8.4	−20.4	1.6	1.0	0.50	11
0.92	158.8	−7.2	−20.3	0.2	0.1	0.61	–

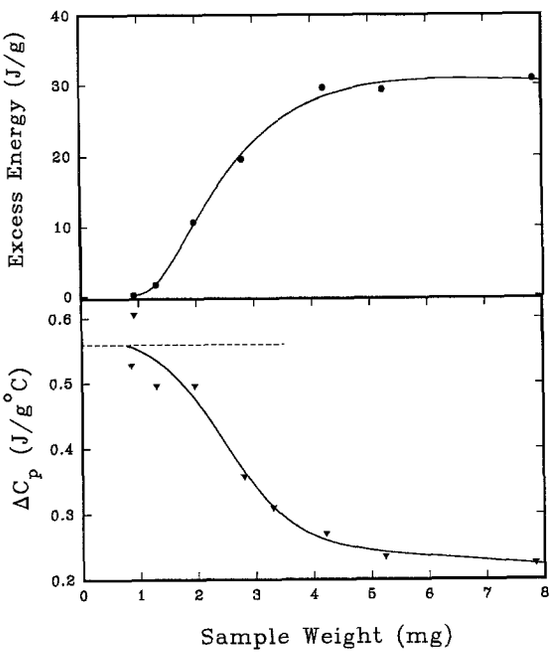

Figure 5 Excess energy between the exothermic and endothermic regions, and ΔC_p, for quench-cooled iPP samples of different weights

The degree of crystallinity that develops during quench cooling can be estimated from the excess energy (defined as the difference between the heat of fusion in the region between 120 and 170°C and the heat of crystallization measured between about −15 and 120°C) as well as from the change in heat capacity at the glass transition using the relationship:

$$w_c = 1 - \frac{\Delta C_p}{\Delta C_p^o} \quad (1)$$

where ΔC_p is the measured change in heat capacity at the glass transition, ΔC_p^o is the corresponding change in heat capacity of the pure amorphous glass ($\Delta C_p^o = 0.559 J g^{-1} °C^{-1}$)[31] and w_c is the weight fraction crystallinity. The degrees of crystallinity derived by these two methods, as well as some of the transition temperatures, are given in *Table 1* for iPP samples with weights ranging from less than 1 to 8 mg.

As seen in *Figure 5*, for sample weights >4 mg, the heat of fusion exceeds the heat of crystallization by about $30 J g^{-1}$. This corresponds to the formation of about 18% crystallinity during sample quenching, based on $165 J g^{-1}$ as the heat of fusion for a 100% crystalline iPP sample[32]. As the sample weight is reduced the excess endothermic energy decreases and approaches zero for sample weights <1 mg. Similarly, the ΔC_p for samples of low mass approaches the accepted value for a 100% amorphous glass (represented by a dashed line in *Figure 5*) but decreases with an increase in sample weight, in keeping with higher crystallinity for the larger sample weights. These observations suggest that quench cooling iPP samples of low mass at rates accessible to these experiments results in essentially amorphous glasses, while samples with higher weights develop some crystallinity. The total sample crystallinity, as judged from the final melting peak, at 158±1°C is constant at $76 \pm 2 J g^{-1}$, which corresponds to a sample crystallinity of 46±2%. This total developed crystallinity is consistent with the results of Fichera and Zannetti[26], who also reported an ultimate heat of fusion of $75 J g^{-1}$, but is slightly higher than a crystallinity of 38±2% reported by Grebowicz *et al.*[27].

As developed above, samples of higher mass show significantly larger excess energies with a concomitant decrease in ΔC_p, reflecting the development of some crystallinity in these samples during quench cooling, while those of low mass show essentially no excess energy and exhibit the ΔC_p expected for a 100% amorphous sample. However, as seen in *Table 1*, the degree of crystallinity obtained from ΔC_p for samples of higher mass is significantly larger than that derived from the excess energy. In fact, the degree of crystallinity estimated from the change in heat capacity exceeds the crystallinity estimated from the final melting peak, which is unrealistic. Two explanations are offered for these discrepancies.

During the quench cooling of samples of higher mass, appreciable crystallinity is developed and, as predicted by equation (1), this diminishes the measured ΔC_p. However, not all of the non-crystalline portion experiences this low temperature glass transition and as a result the degree of crystallinity is overestimated. Indeed, there is much evidence[33–36] from thermal expansion, specific heat and mechanical loss data for two glass-like transitions in bulk crystallized iPP. For iPP samples possessing very low crystallinity, the first or lower glass transition, T_g(L), was reported to lie between −20 and −12°C, while a second or upper glass transition, T_g(U), has been reported to occur from 20°C up to temperatures as high as 100°C. It was suggested that the T_g(L) is associated with amorphous material rejected by the crystallites as well as cilia, while loose loops from chain-folded crystals as well as tie molecules exhibit T_g(U). The unrealistic

crystallinities inferred from ΔC_p at $T_g(L)$ suggest that a portion of the amorphous content of the high mass samples passes through the glass transition at higher temperatures and is undetected because of the other exothermic processes that occur simultaneously. A similar observation was also made by Grebowicz *et al.*[27], who reported that only 10–20% of the amorphous content shows an identifiable T_g in the vicinity of the lower glass transition region.

The second plausible explanation for the discrepancies observed in the estimated crystallinities obtained on quench cooling is based on the nature of the crystalline order obtained when the sample is quench cooled to the glass state. If quench cooling results in the formation of a state of poor crystalline order, the eventual melting of this morphology may require less energy than that for a perfect α-monoclinic crystal (i.e. $< 165\,J\,g^{-1}$). Such a situation would result in an underestimation of the crystallinity on quench cooling as measured from the excess energy. STEM dark field and electron diffraction results presented below reveal the existence of such a poor crystalline fraction.

Solid state n.m.r.

The solid state n.m.r. CP/MAS spectrum of the quench-cooled phase of iPP that has been warmed to room temperature, shown in *Figure 6b*, exhibits resonances for the methylene, methine and methyl carbons at 44.6, 26.7 and 22.1 ppm, respectively, consistent with previously reported spectra for such samples[37–39]. In annealed or isothermally crystallized iPP (i.e. at high temperature), the methylene and methyl resonances show a double peak separated by about 1 ppm, as seen in *Figure 6a* for a quenched sample which was annealed at 161°C for 1 h. It has been postulated that this resonance splitting is a consequence of inequivalent distances within the α-monoclinic unit cell which results from regular packing of right- and left-handed helices. In the case of the quenched iPP, neither the methylene nor the methyl resonance show the type of splitting that is observed for the α-monoclinic crystalline phase. This suggests either that the quenched morphology is not comprised of the α-monoclinic crystal form or that it is composed of an α-monoclinic phase where inequivalent distances within the unit cell do not exist. The latter explanation requires that the interhelical distances in the unit cell be larger than in the stable α-monoclinic crystal form so that inequivalent local sites are not observed.

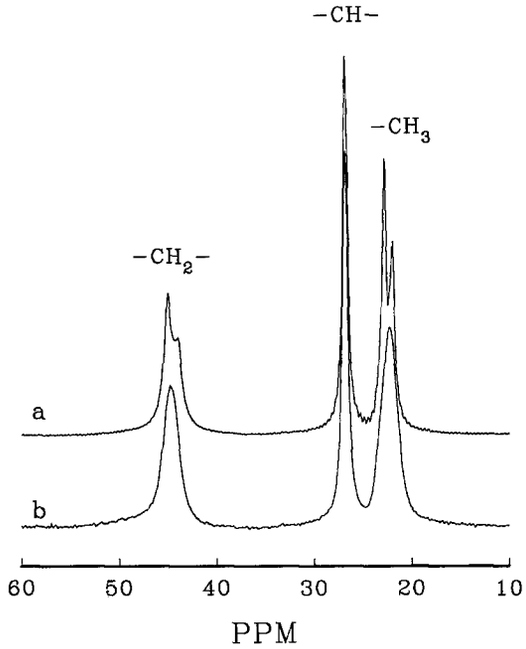

Figure 6 Solid state ^{13}C CP/MAS n.m.r. spectrum for a quench-cooled iPP sample which was (a) annealed at 161°C for 1 h, and (b) allowed to return to room temperature

The measured ^{13}C spin-lattice relaxation times in a rotating frame, $T_{1\rho}(^1H)$, of the quenched morphology consist of two components: a long component of 14.2, 14.8 and 14.1 ms, and a short component of 2.5, 3.7 and 1.8 ms, for the methylene, methine and methyl carbons, respectively. This is in keeping with previous reports by Tanaka[39] who attributed the long component to the relaxations in the crystalline phase while the short component was assigned to the amorphous. By comparison, the relaxation times for an α-monoclinic crystalline phase annealed at 161°C for 1 h consist of a long component relaxation time of 126, 121 and 123 ms, and a short component of 19, 18 and 18 ms. It is well known[37,40] that $T_{1\rho}(^1H)$ is dominated by low frequency motions and that the shorter relaxation times can be ascribed to the more mobile phase. The shorter relaxation times measured for the quench-cooled phase indicate that it possesses higher mobility, hence much lower crystallinity, than the stable α-monoclinic crystalline phase. It is rather interesting that the short relaxation times of the annealed α-monoclinic crystals are rather similar to the long relaxation times for the quenched sample.

The results presented above show that a metastable morphology develops on heating quench-cooled iPP to room temperature, as evidenced by the exothermic nature of the 'as-quenched' thermogram that results on further heating (*Figure 4*). The solid state n.m.r. data for this phase, as well as its thermal behaviour, are consistent with previous reports and indicate that the samples used in this study possess the same morphology as those studied previously by other authors. New information about the nature of this morphology, obtained through the use of electron microscopy techniques offering higher resolution than used previously, will now be presented.

Electron microscopy

The STEM dark-field image of n-beam reflections of the quench-cooled iPP sample that has been returned to room temperature, shown in *Figure 7*, reveals the presence of microcrystalline regions ranging in size from 100 to 200 Å, with an average of 160 Å, as is clearly indicated by the white regions. These crystal sizes were determined using the Scherrer method[41] where the breadth at half-height of a given reflection is related to the crystal size by a geometry-dependent constant as well as through direct measurement on the negative. In addition, the black areas give evidence of amorphous material in which lie regions of a low level of crystalline order, seen as the grey areas between the bright microcrystals. *Figure 8* shows typical micro–micro electron diffractions probing areas less than $100\,Å^2$ in size for each of these three regions. Analysis of the diffraction pattern of the microcrystalline region indicates the existence of the α-monoclinic crystal structure with unit cell constants *a*, *b*, *c* and *β* equal to 6.67 ± 0.01, 20.89 ± 0.05, 6.48 ± 0.01 Å and $98.4 \pm 0.6°$, respectively. These unit cell constants for

Figure 7 STEM dark-field image of n-beam reflections of a quench-cooled iPP sample. Magnification 50 000 × (1 cm = 0.05 μm)

the microcrystalline regions are consistent with previously reported values[9,11,42] for the α-monoclinic crystal form. Based on 12 monomer units per unit cell, the density of this phase corresponds to $0.937 \pm 0.001\ g\,cm^{-3}$, which is also consistent with previously reported values[42].

The intercrystalline regions, i.e. the grey areas, possess unit cell constants which are substantially larger: $a = 7.03 \pm 0.01$, $b = 21.1 \pm 0.1$, $c = 6.47 \pm 0.02$ Å and $\beta = 99 \pm 2°$. These results indicate that the packing of the helices in the intercrystalline region is less compact than in the microcrystalline region, yielding larger interhelical distances and thus a substantially lower density of $0.882 \pm 0.004\ g\,cm^{-3}$. Nonetheless, the α-monoclinic crystal form is still evident. It should be noted that the various reflections observed in the electron diffraction of this region do not show arcs, as seen for the microcrystalline region, which is consistent with lower crystalline orientation in this phase.

The micro–micro electron diffraction pattern of the amorphous regions (*Figure 8c*) observed in the STEM dark-field image gives evidence of some periodicity, even though no scattering is observed in the dark field image. The single reflection indicates that some structure exists within this phase, although it is essentially amorphous. Typical d-spacings with the corresponding Miller indices for all three regions are summarized in *Table 2*.

The typical diffraction patterns obtained by wide-angle X-ray scattering and by conventional electron diffraction

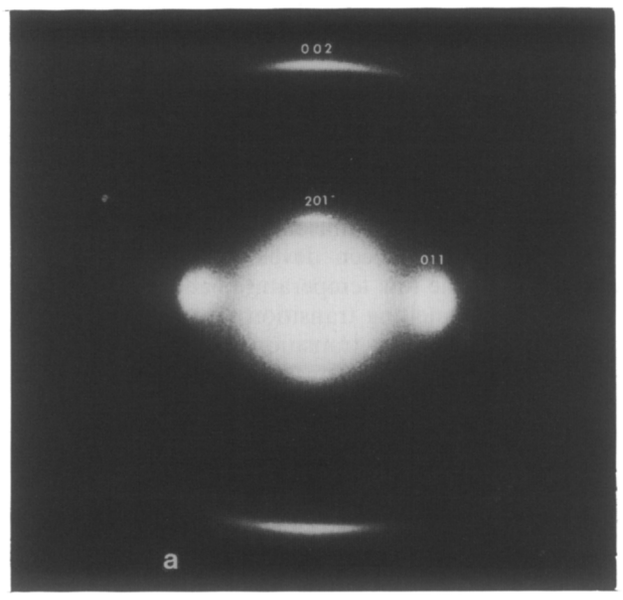

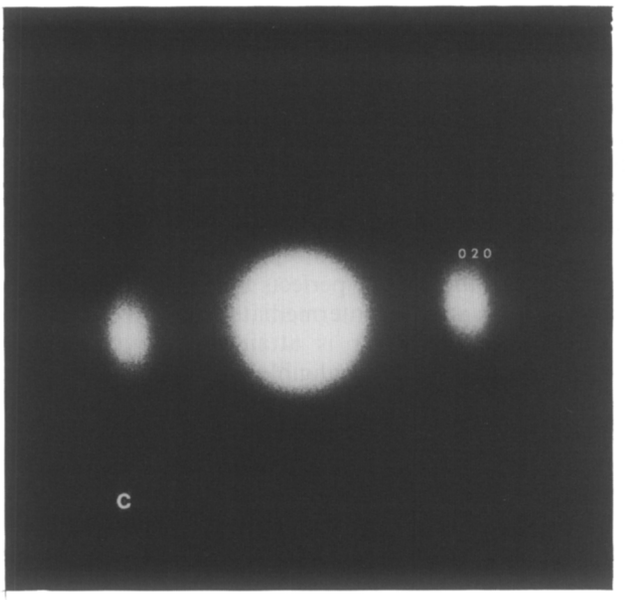

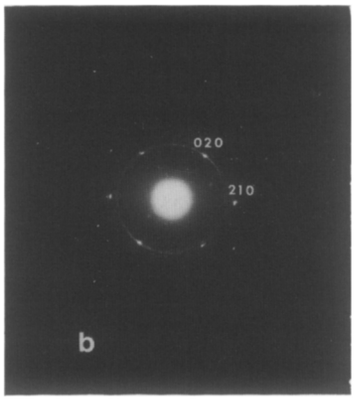

Figure 8 Typical micro–micro electron diffraction patterns of (a) microcrystalline, (b) intercrystalline and (c) amorphous areas

Table 2 Miller indices with corresponding d-spacings of the microcrystalline, intercrystalline and amorphous regions obtained from the micro–micro electron diffraction patterns

	Parallel to face of film		Perpendicular to face of film	
Region	Miller indices (h,k,l)	d-Spacing (Å)	Miller indices (h,k,l)	d-Spacing (Å)
Microcrystalline	002	8.6	231	10.3
	201	4.3	140	9.7
	011	5.4	311	7.8
	101	6.7	312	6.7
Intercrystalline	020	6.71	240	8.65
	100	7.81	330	6.78
	230	6.77	001	5.61
	210	4.32	021	5.56
Amorphous	020	6.41		

therefore reflect a combination of contributions from the three phases of the quenched morphology. Calculations by previous authors[16,20], based on the half-width of the most intense wide-angle X-ray diffraction (WAXD) peak, indicated that the 'smectic' morphology contains crystals ranging in size from 30 to 100 Å. This study shows, by direct measurement, larger crystals having dimensions of the order of 160 Å. Since the crystals are not as small as reported previously, it must be concluded that the sample possesses a great deal of disorder which is causing the WAXD line broadening. The intercrystalline regions of lower crystalline order, as well as the partial order that exists within the essentially amorphous phase, can broaden the WAXD reflections. The intercrystalline region should yield slightly different d-spacings from those of the microcrystals for a given crystal orientation due to the larger unit cell constants of the intercrystalline region. Convolution of the diffractions from the intercrystalline and microcrystalline regions would result in broadened peaks and a featureless diffraction pattern. Annealing at about 60°C perfects both the microcrystals as well as the areas of intermediate order. Eventually a sufficient level of order is attained so that the line broadening effects are negligible and a transformation from the quench-cooled phase diffraction pattern to that of the α-monoclinic crystal form is observed.

In previous transmission electron microscopy studies, Gezovich and Geil[18] observed large spherulite-like structures, about 1 μm in diameter, in surface replicas of thick quenched films, while nodular structures about 125 Å in diameter were seen in very thin quench-cooled films. The latter morphology was interpreted as being the 'smectic' structure and it was suggested that the nodules are defective hexagonal crystals. Similar nodular structures, 75–100 Å in size, were reported for the smectic morphology by Hsu *et al.*[24] although they did not detect the spherulitic structures. They suggested that the main reason for the discrepancy was the difference in the iPP. To determine if these nodular structures are small crystals, dark-field images were attempted; however, the authors were unsuccessful in obtaining such images, which was taken as a confirmation of the small and imperfect nature of the quenched morphology. Using TEM, Grubb and Yoon[43] also observed a nodular morphology, about 200 Å in diameter, in permanganate-etched surfaces of quenched iPP films. This nodular morphology was found to become better defined, with clearer limits and boundaries, when the samples were annealed at 60°C, consistent with a perfection of the intercrystalline regions, as discussed previously. The microcrystalline regions evident in *Figure 7* are consistent in size with the nodular structures observed previously and identified as the 'smectic' morphology.

The discrepancy between the exothermic and endothermic transitions observed in the thermogram for the 'as-quenched' sample, described above, results from the development of low crystalline order during the quenching process, probably of the type seen in the intercrystalline regions in *Figure 7*. This proposal is further supported by the results of Zerbi *et al.*[44] who, on the basis of evidence from infra-red studies, reported the presence of segments at least five PP repeat units in length having helical conformation in iPP melts. Such structure would be 'frozen in' with some additional ordering during the quenching of the sample, and would result in some low level structure such as is observed in the intercrystalline regions (*Figure 7*). Heating the sample to room temperature is accompanied by crystallization from the glassy state. This crystallization, releasing about 18 J g^{-1} between −15 and 25°C, reflects the formation of the microcrystalline regions observed in the STEM dark-field image.

Based on the above considerations, it is unlikely that the low temperature endotherm observed in *Figure 1* is due to melting of small crystals formed during the quenching or subsequent annealing of the iPP sample, as proposed previously by others. The thermogram of the 'as-quenched' sample (*Figure 4*) reveals that about 18 J g^{-1} of crystallinity has developed as the temperature of the sample is raised to room temperature, ignoring the crystallinity developed during the sample quench cooling. By comparison, the area of the low temperature endotherm in *Figure 1* corresponds to 4.4 J g^{-1}, or only 23% of that required to melt the microcrystals. Therefore, the total heat of melting is insufficient to account for the crystallinity that has been developed. It seems more reasonable that the low temperature endotherm reflects some form of premelting transition that occurs prior to recrystallization. Such a transition may involve expansion in one or both dimensions of the crystal lattice in a direction perpendicular to the molecular chain direction. Such an endothermic transition may be a requirement prior to sample recrystallization, which occurs at slightly higher temperatures whereafter factors such as chain-fold length and crystal perfection may increase. It is of interest that this transition is not detected in the thermogram of the 'as-quenched' sample.

The partially ordered phase of iPP has been shown to be composed of microcrystalline as well as intercrystalline regions possessing an α-monoclinic crystal form. Consequently, the small exotherm observed in *Figure 1* certainly does not represent the transformation from a quench-cooled phase morphology to the more stable α-monoclinic crystal form. Rather, it must be regarded as perfection of the existing α-monoclinic crystal form to higher levels of order.

Gomez *et al.*[38], in a high resolution solid state ^{13}C n.m.r. study of iPP polymorphs, inferred the local chain packing structure of the smectic form through comparisons with the n.m.r. spectra of the well known α and β crystal forms. The chemical shifts, as well as the spin-lattice relaxation times, for the smectic form were

found to be similar to those of the β-phase. This similarity led to the suggestion that the packing of the helices in the quenched phase, at least on a very local scale, is similar to the packing in the β-form. In this study it was shown that the quenched iPP morphology is composed of small crystals of the α-phase possessing the same unit cell dimensions as usually reported in the literature. However, the n.m.r. spectrum of the quenched phase does not show the expected characteristics of an α-phase (*Figure 6*). It is possible that due to the presence of the intercrystalline phase, which, as described previously, possesses substantially larger unit cell constants, the inequivalent distances are not being resolved in the n.m.r. experiment. Substantially larger interhelical distances in the intercrystalline phase would obscure the inequivalent distances that are found in the microcrystalline regions. Through annealing, and thus perfection of both phases, it becomes possible to resolve these small differences in interhelical distances and the resonances begin to show the expected splitting observed for an α-phase.

CONCLUSIONS

It has been demonstrated that the morphology of a previously quench-cooled iPP sample that has been heated to room temperature is composed of three phases. (1) Microcrystalline regions that range in size between 100 and 200 Å, having the α-monoclinic crystal form. (2) Regions of lower crystalline order also composed of the α-monoclinic crystal form. The helical packing in this region was found to be much less compact than in the microcrystalline region, as evidenced by larger unit cell constants. (3) An amorphous phase in which, as seen by micro–micro electron diffraction, there exists some periodicity although no scattering was observed in the dark-field image.

The bulk diffraction X-ray or electron diffraction patterns generally obtained for this morphology are consistent with the occurrence of line broadening effects from intercrystalline regions on the diffraction pattern of small α-monoclinic crystals, about 160 Å in size. Annealing samples with this morphology at temperatures above room temperature perfects the crystalline structure in the microcrystalline as well as in the intercrystalline regions, so that the α-monoclinic form is detectable by conventional diffraction techniques due to suppression of the line broadening effects.

The formation of regions of low crystalline order, of the type observed in the intercrystalline regions of the room temperature annealed sample, occurs during the quench cooling of the iPP sample. This is evidenced by the difference in ΔH between the exothermic and endothermic transitions as well as by the changes in ΔC_p observed in *Figure 5*. Quench cooling of an iPP sample of low mass appears to yield an amorphous glass, while larger masses form a glass possessing a low degree of crystallinity (i.e. up to 18%). Raising the temperature of the quench-cooled iPP sample results in crystallization from the glassy state, where the kinetics of crystallization are controlled by chain transport. This crystallization results in the formation of the microcrystals observed in the STEM dark-field image. The resultant morphology is metastable, as evidenced by the fully exothermic d.s.c. thermogram in the region between -15 and 120°C, such that raising the temperature within this region results in the generation of a new crystalline morphology having a higher level of order.

ACKNOWLEDGEMENTS

Financial support in the form of operating grants and scholarships (V.C.) from the Natural Sciences and Engineering Research Council of Canada (NSERC) and the Québec Government (Fonds FCAR) is gratefully acknowledged.

REFERENCES

1 Natta, G., Pino, P., Corradini, P., Danusso, F., Mantica, E., Mazzanii, G. and Moriglio, G. *J. Am. Chem. Soc.* 1955, **77**, 1708
2 Morris, D. R. *J. Macromol. Sci., Phys.* 1969, **B3**(1), 53
3 Keith, H. D., Padden, F. J. Jr, Walker, N. M. and Wyckoff, H. W. *J. Appl. Phys.* 1959, **30**, 485
4 Addink, E. J. and Beintema, J. *Polymer* 1961, **2**, 185
5 Pae, K. D., Sauer, J. A. and Morrow, D. R. *Nature* 1966, **211**, 514
6 Kardos, J. L., Christiansen, A. W. and Baer, E. *J. Polym. Sci. (A-2)* 1966, **4**, 777
7 Lotz, B. and Wittmann, J. C. *J. Polym. Sci., Polym. Phys. Edn* 1986, **24**, 1541
8 Lotz, B., Graff, S. and Wittmann, J. C. *J. Polym. Sci., Polym. Phys. Edn* 1986, **24**, 2017
9 Brückner, S., Meille, S. V., Petraccone, V. and Pirozzi, B. *Prog. Polym. Sci.* 1991, **16**, 361
10 Natta, G., Peraldo, M. and Corradini, P. *Rend. Accad. Naz. Lincei.* 1959, **26**, 14
11 Natta, G. and Corradini, P. *Nuovo Cimento, Suppl.* 1960, **15**, 40
12 Wycoff, H. W. *J. Polym. Sci.* 1962, **62**, 83
13 Miller, R. L. *Polymer* 1960, **1**, 135
14 Zannetti, R., Celotti, G. and Armigliato, A. *Eur. Polym. J.* 1970, **6**, 879
15 Hosemann, R. *J. Appl. Phys.* 1963, **34**(1), 25
16 Gailey, J. A. and Ralston, P. H. *SPE Trans.* 1964, **4**, 29
17 Farrow, G. *J. Appl. Polym. Sci.* 1965, **9**, 1227
18 Gezovich, D. M. and Geil, P. H. *Polym. Eng. Sci.* 1968, **8**, 202
19 Bodor, G., Grell, M. and Kallo, A. *Faserforsch. Textil-Tech.* 1964, **15**, 527
20 McAllister, P. B., Carter, T. J. and Hinde, R. M. *J. Polym. Sci., Polym. Phys. Edn* 1978, **16**, 49
21 Guerra, G., Petraccone, V., De Rosa, C. and Corradini, P. *Makromol. Chem., Rapid Commun.* 1985, **6**, 573
22 Corradini, P., Petraccone, V., De Rosa, C. and Guerra, G. *Macromolecules* 1986, **19**, 2699
23 Corradini, P., De Rosa, C., Guerra, G. and Petraccone, V. *Polym. Commun.* 1989, **30**, 281
24 Hsu, C. C., Geil, P. H., Miyaji, H. and Asai, K. *J. Polym. Sci., Polym. Phys. Edn* 1986, **24**, 2379
25 Glotin, M., Rahalkar, R. R., Hendra, P. J., Cudby, M. E. A. and Willis, H. A. *Polymer* 1981, **22**, 731
26 Fichera, A. and Zannetti, R. *Makromol. Chem.* 1975, **176**, 1885
27 Grebowicz, J., Lau, S.-F. and Wunderlich, B. *J. Polym. Sci., Polym. Symp.* 1984, **71**, 19
28 Vittoria, V. *J. Macromol. Sci.* 1989, **B2**(3), 489
29 De Candia, F., Russo, R. and Vittoria, V. *J. Appl. Polym. Sci.* 1987, **34**, 689
30 Zannetti, R., Celotti, G., Fichera, A. and Francesconi, R. *Makromol. Chem.* 1969, **128**, 137
31 Gaur, U. and Wunderlich, B. *J. Phys. Chem. Ref. Data* 1981, **10**(4), 1051
32 Wunderlich, B. 'Macromolecular Physics, Vol. 3, Crystal Melting', Academic Press, New York, 1980
33 Boyer, R. F. *J. Macromol. Sci., Phys.* 1973, **B8**(3–4), 503
34 Beck, D. L., Hiltz, A. A. and Knox, J. R. *SPE Trans.* 1963, **3**, 279
35 Wada, Y., Hotta, Y. and Suzuki, R. *J. Polym. Sci., Part C* 1968, **23**, 583
36 Jarrigeon, M., Chabert, B., Chatain, D., Lacabanne, C. and Nemoz, G. *J. Macromol. Sci., Phys.* 1980, **B17**(1), 1
37 Bunn, A., Cudby, M. E. A., Harris, R. K., Packer, K. J. and Say, B. J. *Polymer* 1982, **23**, 694
38 Gomez, M. A., Tanaka, H. and Tonelli, A. E. *Polymer* 1987, **28**, 2227
39 Tanaka, H. *Eur. Polym. J.* 1991, **27**(7), 565
40 Schaeffer, J., Stejskal, E. O. and Buchdahl, R. *Macromolecules* 1975, **8**, 291
41 Scherrer, J. *Nachr. Ges. Wiss. Gottingen* 1918, 96
42 Brandrup, J. and Immergut, E. H. (Eds) 'Polymer Handbook' 3rd Edn, John Wiley and Sons, New York, 1989
43 Grubb, D. T. and Yoon, D. Y. *Polym. Commun.* 1986, **27**, 84
44 Zerbi, G., Guzzoni, M. and Ciampelli, F. *Spectrochim. Acta* 1967, **23A**, 301